Environmental Science Nano

Characterization of silver and silver nanoparticle interactions with zinc finger peptides

Journal:	*Environmental Science: Nano*
Manuscript ID	EN-ART-01-2019-000065.R2
Article Type:	Paper
Date Submitted by the Author:	28-Jun-2019
Complete List of Authors:	Park, Grace; Santa Clara University, Chemistry and Biochemistry Amaris, Zoe; Santa Clara University, Chemistry and Biochemistry Eiken, Madeline; Santa Clara University, Chemistry and Biochemistry Baumgartner, Karl; Santa Clara University, Chemistry and Biochemistry Johnston, Kathryn; University of Pittsburgh, Chemistry Williams, Mari; Santa Clara University, Chemistry and Biochemistry Markwordt, Jasmine; Santa Clara University, Chemistry and Biochemistry Millstone, Jill; University of Pittsburgh, Chemistry Splan, Kathryn; Macalester College, Chemistry Wheeler, Korin; Santa Clara University, Chemistry and Biochemistry

Characterization of silver and silver nanoparticle interactions with zinc finger peptides

Grace Park[1], Zoe N. Amaris[1], Madeline K. Eiken[1], Karl V. Baumgartner[1], Kathryn A. Johnston[2], Mari A. Williams[1], Jasmine G. Markwordt[1], Jill E. Millstone[2], Kathryn E. Splan[3], and Korin E. Wheeler[1]*

[1]Department of Chemistry & Biochemistry Santa Clara University Santa Clara, CA 95053, USA.
[2]Department of Chemistry, University of Pittsburgh, 219 Parkman Ave, Pittsburgh, PA 15260, USA.
[3]Department of Chemistry, Macalester College, 1600 Grand Avenue, Saint Paul, Minnesota 55105, USA.
*corresponding author.

Abstract

In the biological systems, chemical and physical transformations of engineered silver nanomaterials (AgENMs) are mediated, in part, by proteins and other biomolecules. Metalloprotein interactions with AgENMs are also central in understanding toxicity, antimicrobial, and resistance mechanisms. Despite their readily available thiolate and amine ligands, zinc finger (ZF) peptides have thus far escaped study in reaction with AgENMs and their Ag(I) oxidative dissolution product. We report spectroscopic studies that characterize AgENM and Ag(I) interactions with two ZF peptides that differ in sequence, but not in metal binding ligands: the ZF consensus peptide CP-CCHC and the C-terminal zinc finger domain of HIV-1 nucleocapsid protein p7 (NCp7_C). Both ZF peptides catalyze AgENM (10 and 40 nm, citrate coated) dissolution and agglomeration, two important AgENM transformations that impact bioreactivity. AgENMs and their oxidative dissolution product, Ag(I)(*aq*), mediate changes to ZF peptide structure and metalation as well. Spectroscopic titrations of Ag(I) into apo-ZF peptides show an Ag(I)-thiolate charge transfer band, indicative of Ag(I)-ZF binding. Fluorescence studies of the Zn(II)-NCp_7 complex indicate that the Ag(I) also effectively competes with the Zn(II) to drive Zn(II) displacement from the ZFs. Upon interaction with AgENMs, Zn(II) bound ZF peptides show a secondary structural change in circular dichroism spectroscopy toward an apo-like structure. The results suggest that Ag(I) and AgENMs may alter ZF protein function within the cell.

Environmental significance

The readily available thiolate ligands in ZFs make them plausible targets to drive AgENM dissolution, resulting in increased release of Ag(I) in cells. In turn, interactions of ZFs with AgENMs and dissolved Ag(I) result in displacement of the native Zn(II) and mediate sequence specific structural changes in ZFs. Because many ZFs serve as transcription factors that control protein expression, the ability of Ag(I) to displace Zn(II) from ZF transcription factors and alter ZF function could have a wide-ranging impact on the overall function of the organism. Ag(I) and AgENM alterations to ZF function constitute a possible toxicity mechanism and may explain sublethal effects of AgENMs in higher level organisms.

Introduction

Due to their antimicrobial properties, silver engineered nanomaterials (AgENMs) are commonly used in consumer goods, including textiles, personal care, kitchen, and medicinal products. The rise in antibiotic resistant infections has increased recent interest in AgENMs in medicinal products in particular. Currently available silver-containing biomedical materials include wound dressings, endotracheal tubes, and bone prostheses.[1] AgENMs are attractive for further development in such biomedical devices where risks of chronic infection are high. Compared to the ionic form, the particle form of silver promises stabilization of silver and controlled release of Ag(I). Yet, the predictable release of Ag(I)(*aq*) from products is complicated by the many variables that control oxidative dissolution of AgENMs, including surface morphology, chemical stabilizers or coatings, shape, size, and biomolecules in solution.[2]

Toxic concentrations of silver are significantly higher in eukaryotes than prokaryotes, thus providing a therapeutic window for antimicrobial treatments. To ensure safe use and inform targeted design of AgENMs, recent studies have elucidated antimicrobial mechanisms,[3,4] as well as eukaryotic response to AgENMs.[4,5] AgENM toxicology has been reviewed and exposure studies have begun to highlight key response mechanisms, including the importance of AgENM oxidative dissolution and use of detoxification pathways known for other, higher abundance metals.[6] For example, upon chronic exposure to AgENMs, rodents accumulated silver ions (not particles) in their livers and biliary systems, then detoxified the silver via a copper pathway.[7–9] Similarly, long-term, low level exposure of AgENMs in fruit flies led to disruption of nonessential copper metalloproteins.[10] These *in vivo* studies of AgENMs highlight the importance of evaluating silver interactions with eukaryotic metalloproteins to elucidate the role of silver in biochemical pathways.

The oxidative dissolution of AgENMs makes it nearly impossible to study the biochemistry of the particle alone. Surface oxidation and silver dissolution are key to most AgENM transformations in biochemical system (reaction 1).

$$2Ag(s) + \tfrac{1}{2}\, O_2(aq) + 2H^+ \rightarrow 2Ag(I)(\text{absorbed}) + H_2O(l) \rightleftharpoons 2Ag(I)(aq) + H_2O(l) \qquad [1]$$

Surface oxidation and silver dissolution are key to most AgENM transformations in biochemical systems. Studies of AgENMs in an aerobic system must then include an analysis of both the particulate zerovalent silver (Ag(*s*)) and oxidized silver (Ag(I)), which is found in greatest abundance in solution after dissolution (Ag(I)(*aq*)). In complex biological systems, the oxidized silver can drive forward additional AgENM transformations through formation of insoluble silver salts, ligation to silver-bound biomolecules, and reoxidation.[11,12] The ligation of silver can catalyze AgENM dissolution, while reoxidation drive reformation of new AgENMs.

Silver ligation is often driven by soft bases such as thiolates and may displace essential metals such as copper or zinc in the process. A small library of metalloenzymes has been studied for their interaction with Ag(I) and AgENMs, including the redox protein Cu(II) azurin,[13,14] two proteins involved in metal homeostasis (metallothionein 1 and periplasmic ceruloplasmin),[15,16]

and the firefly oxidase luciferase[17]. In each case, protein function was disrupted to varying degrees. Even non-metalloproteins have been shown to interact with and drive oxidative dissolution of AgENMs.[18,19] As highlighted by Liu et al,[15] the common feature of these proteins lies in the presence of near-surface ligands, such as cysteine or histidine, available for binding to Ag(I) from AgENMs.

Zinc fingers (ZFs) are a large class of metalloproteins that serve as signaling proteins by binding Zn to surface exposed sites rich in cysteines and histidines.[20–22] ZF proteins undergo a structural change when they bind Zn(II) ions. Ubiquitous in eukaryotes, ZFs serve a variety of roles in the cell, including DNA recognition, RNA packaging, regulation of apoptosis, and protein ubiquitination. Despite the preferred coordination for Zn(II), ZF proteins have shown an affinity for other metals, including Fe(II)[23,24], Ni(II)[24,25], Co(II), Au(I)[26,27], Cu(I)[28–30], Cd(II)[31,32], and Pb(II)[33]. The latter heavy metals have been shown to result in a loss of protein function and provide insight into the toxic properties of Cu(I)[28–30] and Pb(II)[33], for example, and the therapeutic properties of Au(I)[26,27]. Indeed, several ZF proteins were identified in the characterization of the protein coronas of AgENMs formed from yeast proteins[34] and in human blood plasma.[35] Despite the importance of ZF proteins and their known interactions with an array of metals, ZF proteins have not yet been studied in reaction with Ag(I) or metal ENMs.

While it is accepted that Zn(II)-bound form predominates under cellular conditions, cellular metalation state in general is very difficult to assess. Moreover, multiple examples of cell signaling via transition metal ions suggests that metalloprotein metalation state may be more dynamic than initially thought.[36,37] Thus, one can envision that both apo- and Zn(II)-bound ZFs may be found in a cell, depending on cellular concentrations of Zn(II) at a given moment. In response to cell signaling events, concentrations of Zn(II) increase in the cell, which in turn drives Zn(II) binding to apo-ZFs. The Zn(II)-bound ZFs, which have a dramatically different structure than apo-, now serve as a site-specific cellular interactor (e.g. interacting with other proteins, DNA, or RNA to regulate their activity). Thus, to assess the role of a non-native metal on ZF protein function, both apo- and Zn(II) bound structures should be studied.

In this report, we study Ag(I) and AgENM interactions with two model ZF peptides. The two well-characterized ZF peptides vary in length and secondary structure but retain the same four amino acids in the metal binding site, CCHC (**Figure 1**). The longer peptide is a consensus peptide, CP-CCHC, and is representative of the classical ββα ZF fold.[24,33,38,39] The shorter peptide represents the C-terminal ZF domain (residues 34-51) of nucleocapsid protein p7 (NCp7) from the human immunodeficiency virus type 1.[40–43] By comparing these two different ZF peptides, we gain insight into the role of ZF primary and secondary structure in mediating interaction with Ag(I) and AgENMs.

The goal of this study is two-fold. First, we aim to evaluate how the interaction of ZFs with the surface of 10 and 40 nm citrate coated AgENMs and their potential to mediate particle transformations, including agglomeration and oxidative dissolution. Second, we aim to assess structural and functional changes to ZFs as a result of AgENM interactions, including displacement of the native Zn(II) and Ag(I) binding. Because both the apo- and Zn(II) bound

forms of ZFs are biologically relevant, we evaluate both forms in this study. Moreover, by comparing two different ZF peptides and Ag ENM sizes, we also gain insight into the role of peptide and AgENM structure in facilitating interactions and structural changes in both species.

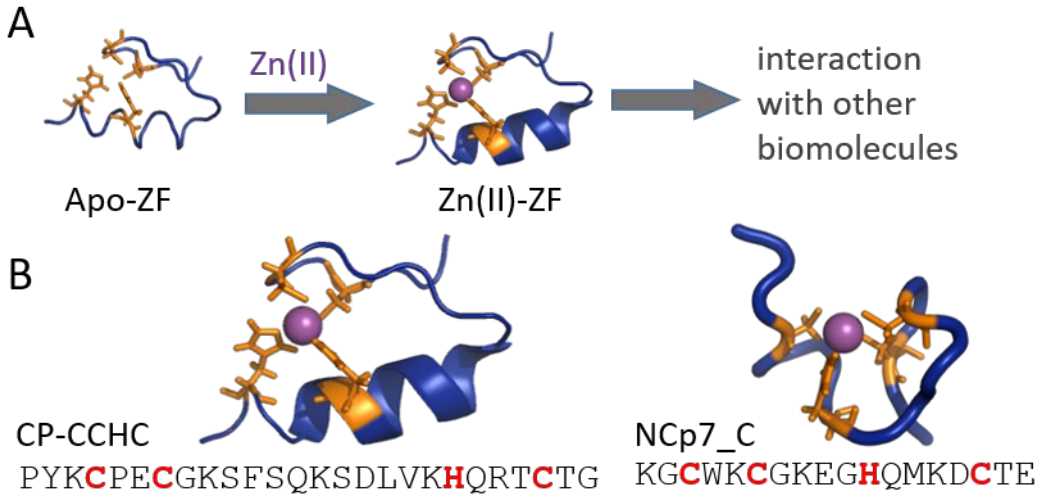

Figure 1. Schematic for ZF reactivity and structures for the model ZF peptides, NCp7_C and CP-CCHC. (A.) Apo-ZFs undergo a dramatic structural change as they bind Zn(II) (shown in purple). In the zinc-bound form, Zn(II)-ZFs can site-specifically interact with DNA, RNA, and other proteins to regulate cellular processes. Graphics of ZFs are for the single metal binding peptide CP-CCHC (modified from PDB ID 2YTR); ZF proteins typically contain several zinc binding domains. For simplicity, apo-ZF graphic shown here is simply a variation of the Zn-bound structure, since apo-ZFs are relatively unstructured and do not have a PDB model available. **(B.)** Two model ZF peptides, CP-CCHC and NCp7_C, were used in this study. Three dimensional structures with secondary elements are shown in blue (modified from PDB ID 2YR for CP-CCHC and 2L44 for NCp7_C), Zn-binding amino acids in orange, and Zn shown as a purple sphere. The primary amino acid sequences are below the 3D structural models, with Zn-binding residues shown in red.

2. Methods

2.1. Sample preparation

Peptides (Bio-Synthesis Inc., > 70% purity) were reduced and further purified in house via reversed-phase high performance liquid chromatography (HPLC). Reduction was performed by incubating peptides with 2 equivalents dithiothreitol per cysteine at 65 °C for 2 hours to reduce thiols. After HPLC purification, samples were immediately lyophilized to dryness and stored at -80 °C. All further measurements were performed in an anaerobic chamber (MBraun) maintained at 90% N_2/10% H_2 unless otherwise noted. Peptide concentrations were calculated from the free thiol content determined by reaction with 5,5-dithiobis-(2-nitrobenzoic acid) (DTNB) to yield TNB^{2-} (ε_{412}=14,150 M^{-1} cm^{-1}).[44]

Zn(II) stock solutions were dilutions of a Zn atomic absorption standard (15.29 mM in 2% HNO_3). Silver stock solutions consisted of 0.1 M $AgNO_3$ (Fluka Analytical). All buffers and stock solutions were prepared with Milli-Q purified water that had been passed over Chelex resin (Sigma) to remove trace metal ion contaminants.

Citrate coated 10 and 40 nm AgENMs stocks were used as received (Biopure from nanoComposix, CA USA). ENMs were characterized before and after peptide exposure. Concentrations of AgENMs are reported here in particle molarity, not total concentration of silver. In this way

2.2. ENM characterization

For Z-average hydrodynamic diameter and zeta potential measurements (ZetaPlus from Brookhaven Laboratories), peptide and AgENMs were reacted in 5 mM citrate in a glovebox. Peptide and AgENM concentrations were determined by the ratio of peptide to AgENMs used in CD experiments. Measurements were taken after 10 minutes of incubation. A Smoluchowski model was used to calculate zeta potential from electrophoretic mobility measurements.

For transmission electron microscopy (TEM) imaging, 20 μM peptide was reacted with 6.7 and 0.42 nM 10 and 40 nm AgENMs (respectively) under anaerobic conditions for 1 hour. Then, 1 uL of sample was drop cast onto a Formvar-coated copper TEM grid. Samples were allowed to air dry and subsequently dried vacuum overnight before characterization using a Hitachi H-9500 environmental TEM at 300 kV (NanoScale Fabrication and Characterization Facility, Petersen Institute of NanoScience and Engineering, Pittsburgh, PA). AgENM size distributions were determined from TEM images of at least 300 NPs from various areas of the grid. Image J 1.47d (National Institutes of Health, USA) was used to measure and count all particles.

2.3. ICP-MS

Concentrations of peptide were 50 μM and 3 nM AgENMs. Samples were centrifuged (30 min, 21 K RCF) to remove ENMs from solution after 6 h incubation. Then, 85 % of the supernatant was removed and recentrifuged to ensure all AgENMs were pelleted out. The sample was then analyzed for Ag(I) concentration.

Ag(I) concentration was determined using an Agilent 7500CE ICP-MS (Agilent Technologies, Palo Alto, CA, USA) by the Interdisciplinary Center for Plasma Mass Spectrometry (University of California at Davis, CA, USA). The samples were introduced using a MicroMist Nebulizer (Glass Expansion, Pocasset, MA, USA) into a temperature-controlled spray chamber. Instrument standards diluted from Certiprep 2A (SPEX CertiPrep, Metuchen, NJ, USA) encompassed the range 0, 0.5, 1, 10, 50, 100, 200, 500, 1000 parts per billion (ppb) in 3 % trace element grade HNO_3 (Fisher Scientific, Fair Lawn, NJ, USA) in 18.2-MΩ water. A separate 100 ppb Certiprep 2A standard was analyzed as every tenth sample as a quality control. Sc, Y, and Bi Certiprep standards (SPEX CertiPrep) were diluted to 100 ppb in 3 % HNO_3 and introduced by peripump as an internal standard.

2.4. UV-vis titrations

Absorption spectra were recorded with a Shimadzu UV-1800 UV-vis spectrometer located within a glovebox to maintain an anaerobic environment. To measure Ag(I) binding to apo-peptides, absorption spectra were recorded after each addition of 0.1 equivalents of metal to a 60 μM ZF peptide sample. Samples were equilibrated for 15 minutes after each metal addition, when no further spectral changes were observed. The spectrum of the corresponding apo peptide was subtracted from the all titration spectra.

2.5. FluoZin studies

Displacement of Zn(II) by Ag(I) was monitored using the zinc-specific probe FluoZin-3 (Invitrogen). Solutions of 50 nM FluoZin-3 and 150 nM Zn(II)-bound peptide were prepared in septum-sealed cuvettes under anaerobic conditions. The solutions were removed from the glove box, and the fluorescence intensity at 520 nm was recorded on excitation at 495 nm. Degassed solutions of aqueous silver nitrate or AgENMs were then added via a gastight syringe, samples were allowed to equilibrate for at least 15 minutes, and the fluorescence was recorded. Control solutions of 50 nM FluoZin-3 with one of the following were also measured to ensure none of the reactants caused interference with the fluorescence signal: 125 nM Zn(II), 150 nM Ag(I), 150 nM apo-peptide, 0.0187 nM 10 nm AgENMs, and 0.001165 nM 40 nm AgENMs were also measured as controls.

2.6. CD studies

Circular dichroism (CD) measurements were performed at 24°C with an Olis RSM 1000 CD spectrometer using a quartz 1 mm pathlength gas-tight cuvette. CD samples were prepared in 10 mM tris(hydroxymethyl)aminomethane buffer, pH 7.5 for a final peptide concentration of 20 μM within a glovebox (MBraun), then sealed with a septum to retain an anaerobic environment during data collection. To test for the displacement of Zn(II) with silver species, the following were added to samples of 20 μM Zn(II) bound peptide, then allowed to react for 20 min prior to taking a spectrum: 44 μM $AgNO_3$, 6.7 nM 10 nm AgENMs, or 0.42 nM 40 nm AgENMs. Three scans were averaged per sample.

3. Results and discussion

3.1. Characterization of AgENMs upon interaction with ZF peptides.

AgENMs are unstable and transform in biological conditions. ZF peptide mediated transformations to the AgENMs may include: a.) interaction at the AgENM surface, b.) agglomeration of the AgENMs, c.) catalysis of AgENM oxidative dissolution, and d.) reformation of AgENMs. These changes to AgENM chemical reactivity, stability, morphology, and size are each strongly correlated with AgENM environmental fate, bioavailability, and toxicity.

3.1.a. Interaction of ZF peptides at the AgENM surface.

To assess interaction of ZF peptides at the AgENM surface, the zeta-potential of the AgENMs was characterized before and after addition of ZF peptides (**Figure 2A**). The strongly negative zeta-potentials for the 10 and 40 nm AgENMs is consistent with their negatively charged citrate coating. Upon addition of apo- or Zn(II) bound ZF peptide, this negative zeta-potential becomes

less negative or positive; this significant shift in zeta-potential upon addition of ZF peptides is indicative of peptide absorption to the particle surface.

When evaluating the zeta-potentials upon addition of apo-peptide, there are minor differences between the two ZF peptides. For 10 nm AgENMs, the CP-CCHC increases zeta-potential more than NCp7_C, which reflects the greater positive charge of the CP-CCHC peptide (pI of CP-CCHC is 8.7 vs 7.1 for NCp7_C). In fact, in the case of 10 nm AgENMs, the zeta-potential is even positive after the addition of CP-CCHC. The differences in apo-peptide zeta-potentials were less pronounced with the 40 nm AgENMs.

Upon addition of Zn(II)-bound ZFs, the zeta potential further increases and, in all cases, becomes positive. This is consistent with the increase in charge to the peptides upon addition of a divalent cation.

3.1.b. Agglomeration of AgENMs upon addition of ZF peptides.

AgENM agglomeration and stability were characterized in solution before and after interaction with ZF peptides to assess changes to AgENM stability. Effective diameters and polydispersity indexes are shown in **Table 1**. Upon addition of ZF peptides, the measured effective diameter of AgENMs increases and results in polydisperse particles. Both 10 and 40 nm AgENMs form significant aggregates upon addition of both apo- and Zn(II)-bound ZF peptides. The agglomeration of AgENMs upon addition of proteins or peptides is common and may be due to a broad range of mechanisms (e.g. protein unfolding, shielding of the AgENM charge, etc). Indeed, the deformability of proteins has been linked to ENM agglomeration[45] and ZF peptide structural changes may, indeed, be the driving force here as well (vide infra). Further research is required to elucidate a detailed mechanism of agglomeration.

3.1.c. ZF peptide catalysis of AgENM oxidative dissolution.

Oxidative dissolution is a well-established chemical transformation of AgENMs in biologically and environmentally relevant systems. Since the bioavailability and toxicity of AgENM is, in large part, due to Ag(I), the oxidative dissolution of AgENMs is particularly relevant for the biological response. The oxidative dissolution of AgENMs was measured with and without the presence of ZF peptides after six hours of reactivity. Then, the AgENMs were spun out of solution and Ag(I)(*aq*) concentrations in the supernatant were measured with ICP-MS. Results of this analysis are shown in **Figure 2B.**

Since AgENMs naturally undergo oxidative dissolution, there is a small amount of dissolved silver in the peptide-free samples. Yet, when ZF peptides are added, the amount of dissolved silver observed in solution was two orders of magnitude higher. This dramatic increase in AgENM oxidative dissolution was consistent across both 10 and 40 nm AgENMs and across apo- and Zn-bound peptides. The largest percentage of Ag(I)(*aq*) detect is a small fraction of the total silver in the sample – at less than 5 %. Thus, although the ZF peptides mediated oxidative dissolution, none of the samples demonstrate a large amount of oxidative dissolution under these reaction conditions. Previous work in AgENM oxidative dissolution suggests that oxidation and release of Ag(I) initially occurs rapidly, or as a “burst”, then slows at later timepoints as the

system reaches solubility limits.[46,47] This type of phenomenon could explain the lower overall concentrations of Ag(I) released across all samples.

Although there is not a clear trend in Ag(I) concentrations measured upon addition of the two different peptides, NCp7_C and CP-CCHC, the peptide conformation appears to influence the dissolution of AgENMs. Dissolution with the addition of Zn(II) bound peptides was higher for seven of the eight samples analyzed with peptide; the sole exception is Zn(II) CP-CCHC in reaction with 10 AgENMs, where measured Ag(I) concentrations were equivalent or slightly lower than apo- CP-CCHC. There may be many mechanistic explanations for this increase in dissolution upon metalation of the peptide. The zeta-potential results, however, suggest that there may be stronger electrostatic interactions between the Zn(II)-bound peptide and the citrate coated AgENMs. The greater ZF peptide- AgENM interaction may, at least in part, lead to increased oxidative dissolution and release of Ag(I) into solution.

The observation that proteins can catalyze oxidative dissolution of AgENMs is in agreement with previous studies that include both metallo-[14–16,48] and nonmetallo-proteins[18,19]. Across these AgENM dissolution studies, the results indicate that exposed metal binding amino acids, like cysteines and histidines, bind dissolved Ag(I) to drive the oxidative dissolution process. Indeed, Marchioni et al demonstrated a correlation between the number of exposed thiols and rates of AgENM dissolution.[48] Other amino acids, such as methionine, may, however, also play a role in the mechanism. For example, in other Ag(I) binding peptides involved in Ag-resistance in bacteria, methionine and histidine appear to play a key role in Ag(I) binding.[49] Protein binding to Ag(I), either from the ENM surface or from solution, would be sufficient to catalyze oxidative dissolution. The theory that thiols, in particular, mediate AgENM dissolution is consistent with the broader argument that sulfidation plays a key role in AgENM transformations, either in biological or environmental systems.[50,51]

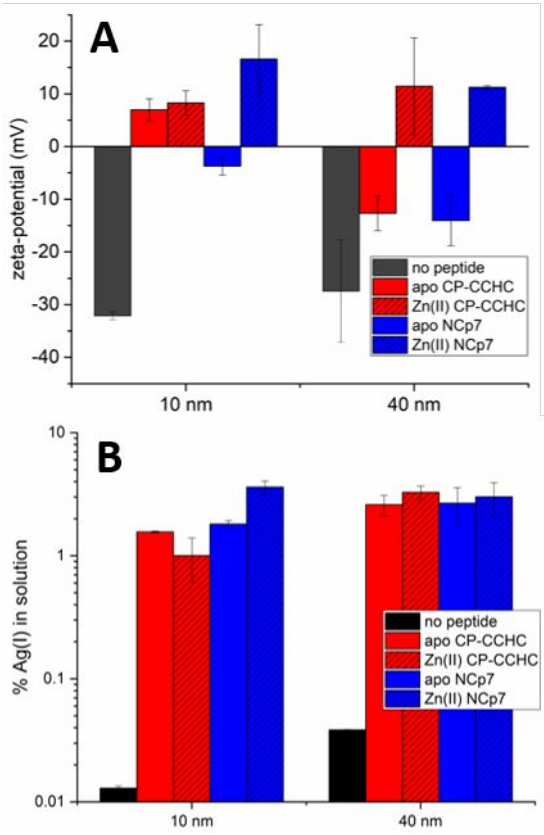

Figure 2. Characterization of 10 and 40 nm AgENMs upon interaction with ZF peptides. **(A.)** Zeta potential of AgENMs with and without ZF peptides was measured in aqueous solution. **(B.)** The percent of total silver in the AgENM sample that has oxidized and dissolved to form Ag(I)(*aq*) was measured in supernatant by ICP-MS after six hours of ZF peptide exposure. Note, the y-axis for the dissolution data is shown on a log-scale to ease comparison across all samples.

Table 1. Effective diameter of AgENMs with and without ZF peptides. Polydispersity is shown in parentheses.

	10 nm AgENMs	**40 nm AgENMs**
no peptide	18.5 (0.163)	45.7 (0.184)
apo NCp7_C	96.6 (0.281)	219.1 (0.266)
Zn(II) NCp7_C	152.2 (0.182)	147.7 (0.332)
Apo CP-CCHC	114.0 (0.222)	282.8 (0.343)
Zn(II) CP-CCHC	180.1 (0.217)	163.7 (0.315)

3.1.d. ZF peptide induced AgENM size or morphology

Previous studies evaluating peptide-AgENM interactions and sulfidation have shown AgENM agglomeration, oxidative dissolution[52] and, in some cases, that the dissolved Ag(I) can reform new AgENMs and may drive oxidative coupling between peptides.[11,12] To evaluate potential reformation of AgENMs and any other changes to AgENM size or morphology, the samples were examined by TEM (**Figure 3**). Consistent with DLS results, some agglomeration appears in the microscopy images of the AgENMs.

Overall, ZF peptide exposure did not change the shape or size of the primary AgENMs. The sizes for the 10 nm AgENMs are: 11.0 ± 2.0 nm, 10.5 ± 2.1 nm, and 10.8 ± 2.1 nm for the AgENMs exposed to NCp7, CP-CCHC, and no peptide, respectively. The sizes for the 40 nm AgENMs are: 36.2 ± 3.8 nm, 36.4 ± 3.7 nm, and 35.8 ± 3.8 nm for the AgENMs exposed to NCp7, CP-CCHC, and no peptide, respectively. Histograms of TEM size measurements are included in the SI (**Figure SI.1**). The 10 nm AgENM samples clearly contained smaller particles in the samples, but the smaller particles do not appear more abundant in the ZF peptide exposed samples.

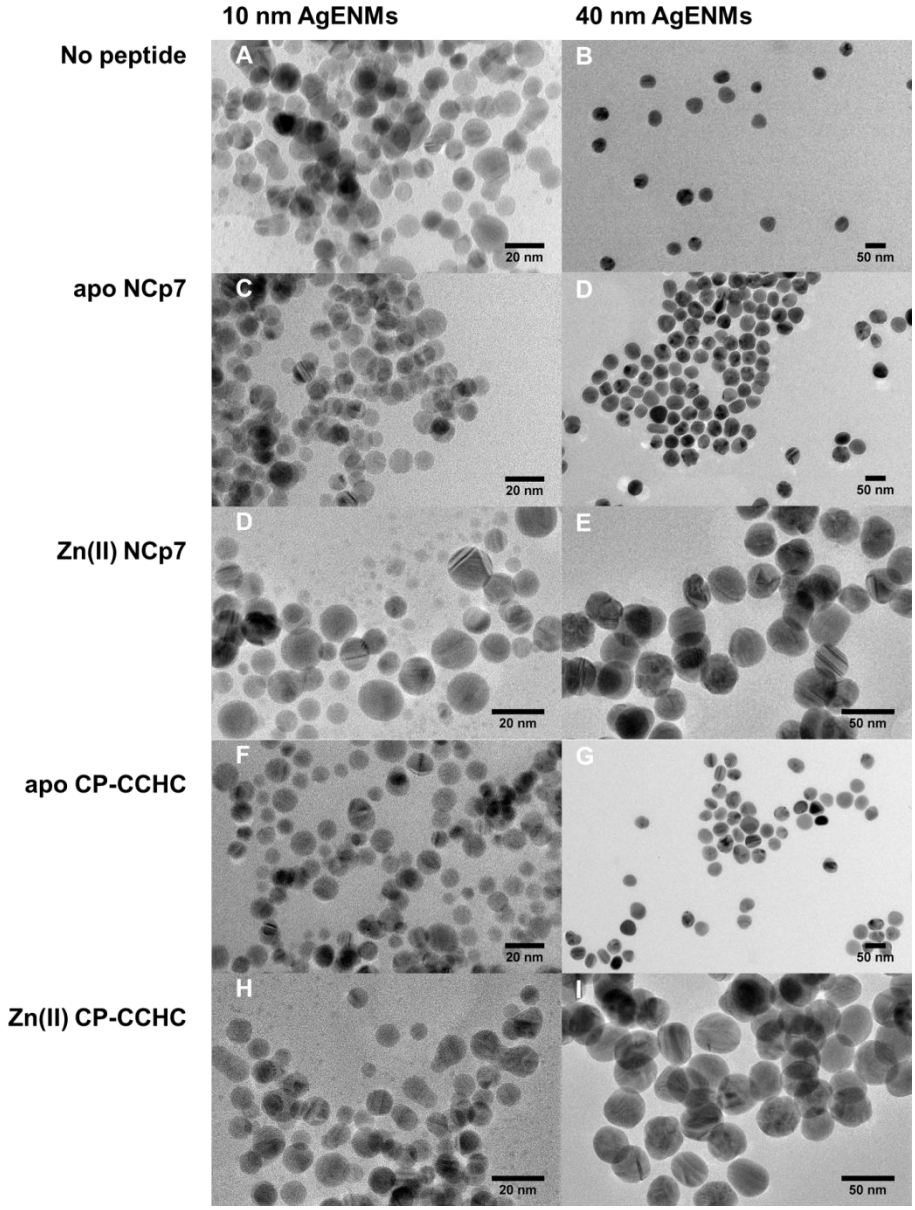

Figure 3. Representative TEM images of AgENMs before and after ZF peptide interaction. Samples at the left (A, C, E, G and I) all contain 10 nm AgENMs and to the right (B, D, F, H and J) contain 40 nm AgENMs. The AgENMs in the top row (A & B) have not been reacted with

peptide; second row (C & D) reacted with apo-NCp7_C; third row (E & F) reacted with Zn(II) NCp7; fourth row (G & H) reacted with apo- CP-CCHC; and bottom row (I & J) reacted with Zn(II) CP-CCHC.

3.2. Ag(I) and AgENM induced changes to ZF peptides

In response to cellular signals that dramatically increase concentrations of Zn(II), ZF proteins respond by binding Zn(II), undergoing a dramatic structural change, and interacting with downstream biomolecules such as DNA. AgENMs, or their oxidative dissolution product Ag(I), may disrupt ZF protein function by: a.) binding to the apo-form of the ZF, b.) disrupting binding of the native Zn(II), or c.) altering the ZF structure to interfere with downstream interactions with other biomolecules.

3.2.a. Ag(I) binding to the apo-peptide

Although metal binding properties of ZF peptides have been widely studied, none have yet focused on Ag(I) binding to ZF peptides. To assess whether ZF peptides bind Ag(I), Ag(I) titrations into ZF apo-peptides were monitored with UV-vis spectroscopy. For both CP-CCHC and NCp7_C, addition of Ag(I) resulted in the appearance of absorption features in the ultraviolet region (**Figure 4**). Unfortunately, AgENM absorbance obscures the ZF peptide spectral features, making it difficult to monitor metal binding to the peptide using electronic spectroscopy. Thus, although titrations of Ag ENMs into apo- ZFs were attempted, results are uninterpretable (data not shown).

Both ZF peptides show high energy transitions that are partially obscured by Ag-citrate buffer interactions along with weaker, lower energy features > 240 nm. For CP-CCHC the high energy feature is centered at 218 nm, with a wide shoulder and secondary feature around 270 nm; similarly, the NCp7_C feature is centered at 233 nm. To ensure these spectral characteristics are not simply a byproduct of Ag(I) binding to the citrate buffer, Ag(I) titrations were also performed in the buffer alone and for each ZF peptide in just water (**Figure S.I.2**). The spectral characteristics observed in for both ZF peptides resemble absorption features previously reported for Ag-metallothionein complexes[16] and are tentatively assigned to Ag(I)-thiolate charge transfer because of its similarity to the same spectral feature previously seen for apo-ZF binding to Cu(I) and other heavy metals[26,28,33]

The increase in absorbance as a function of the number of Ag(I) equivalents at multiple wavelengths indicates that the peptides bind multiple Ag(I) ions per peptide. For both peptides across peaks, absorbances continue to increase beyond the 1:1 stoichiometry of Ag ions to ZF peptide, only leveling out at or above 6 equivalents of Ag(I). The absorbance bands and high concentration of Ag(I) required to reach maximum absorbance is consistent with previous reports of silver binding to metallothionein.[16] The increase in absorbance beyond a 1:1 stoichiometry could be due to weak binding, an alteration of the Ag(I) coordination geometry at higher Ag(I) equivalents, and/or the formation of intermolecular interactions.[28,53] Similar results were reported across an array of heavy metals studied in reaction with ZF peptides.[26,28,33] Although the exact nature of binding is beyond the scope of this report, further study could

elucidate the speciation of these complexes including quantification of silver ions bound to the ZF peptides with LC-MS. Additional methods such as NMR spectroscopy could also provide a structural model of the Ag-bound peptide and may identify the amino acids involved in Ag-binding; however, many of the Ag-binding scenarios mentioned, such as the larger than 1:1 binding stoichiometry and inter-peptide interactions, may complicate spectral interpretation.

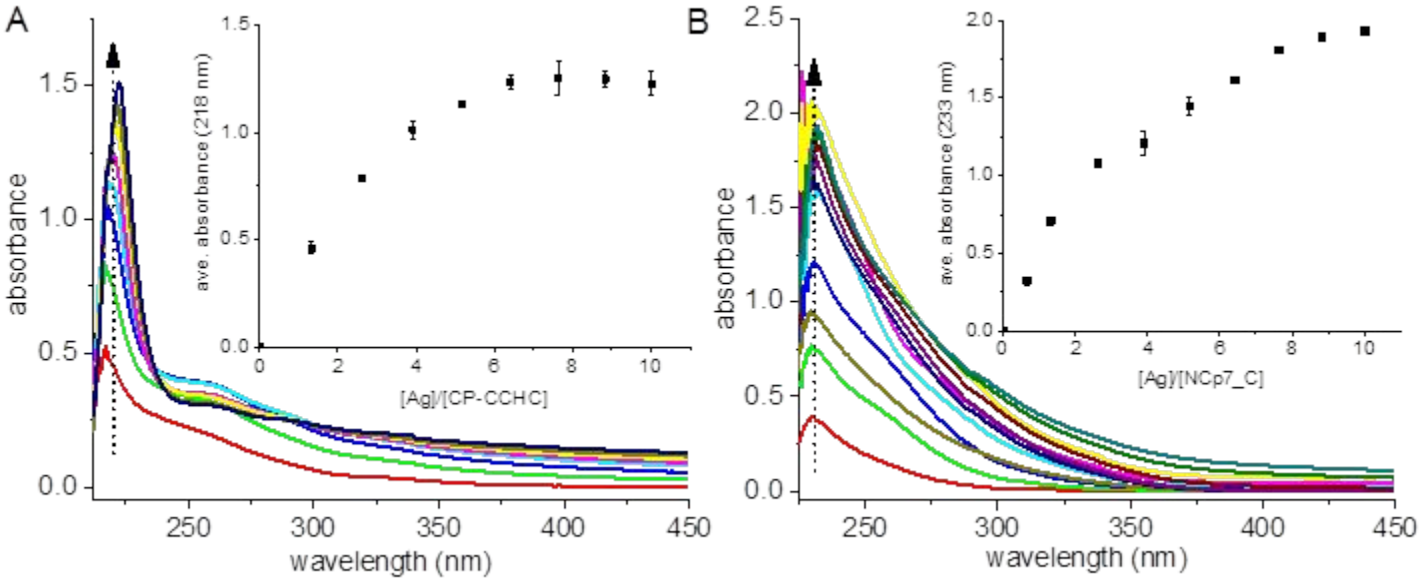

Figure 4. Differential absorption spectra on the addition of Ag(I) to the apopeptides: CP-CCHC (A.) and NCp7_C (B.). Inset shows increase in differential absorbance at 218 nm as Ag(I) was titrated into CP-CCHC **(A.)** and at 233 nm as $AgNO_3$ was titrated into NCp7_C **(B.)**. Arrows in the main figures correspond to the inset. Spectra were recorded with 60 μM peptide in 5 mM citrate buffer at pH 6.2. The apopeptide spectra were used as baselines to give differential absorption as Ag(I) was titrated into the sample. The data are representative of three independent experiments; error bars in the insets show standard deviation across the trials.

3.2.b. Ag(I) binding to the Zn(II) bound peptide

The effects of silver ions on the Zn(II) bound ZF peptides was also monitored. Induced changes to the Zn(II) bound ZF structure of NCp7_C were confirmed and quantified using the intrinsic fluorescence of tryptophan (position 37) in NCp7_C (**Figure 5**). Consistent with earlier reports, intrinsic tryptophan fluorescence increases considerably upon Zn(II) binding to the apo-peptide.[28,43] Addition of Ag(I) and AgENMs result in quenching of the tryptophan fluorescence. For Ag(I), quenching begins to level off near two equivalents of Ag(I). The quenching of tryptophan's intrinsic fluorescence in Zn(II) NCp7_C with just two equivalents of Ag(I) suggests the loss of Zn(II) and structural changes upon Ag(I) binding.

Although Ag ENMs, both 10 and 40 nm in size, were tested, the inner filter effects from the particles' strong absorption at excitation and emission wavelengths hindered our ability to collect reliable data with AgENMs.

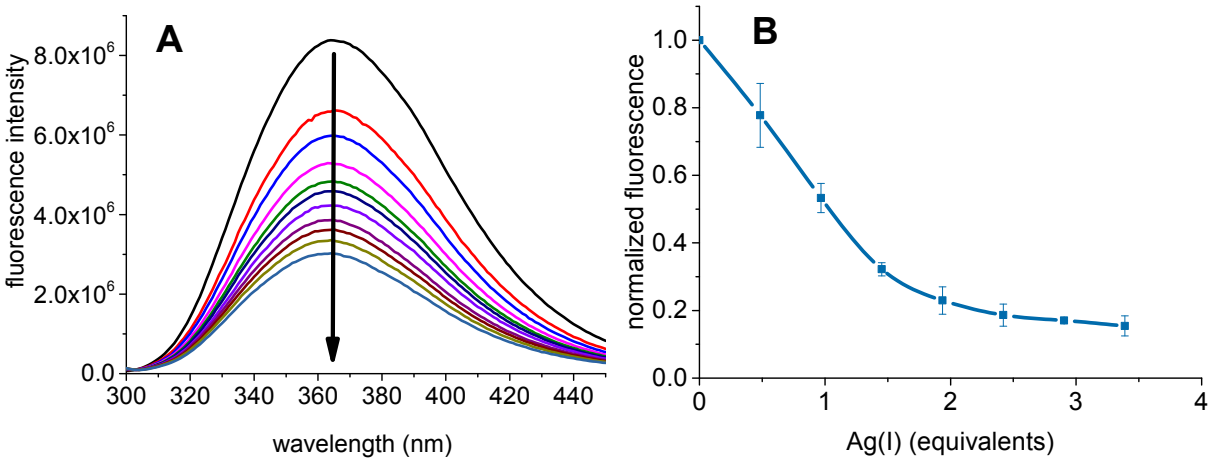

Figure 5. Intrinsic fluorescence spectra (λ(ex) = 280 nm) of 40 μM Zn(II) NCp7_C upon addition of Ag(I). (A.) Sample fluorescence spectra of Zn NCp7_C (black line) upon addition of $AgNO_3$ (all other spectra). **(B.)** Normalized fluorescence intensity (λ(em) = 364 nm) during the titration of Ag(I). Spline curve is provided to guide the eye and is not a fit of the data.

3.3 Ag(I) and AgENM displacement of the native Zn(II) bound to ZF peptides

The loss of bound Zn(II) from ZF peptides is key to evaluating the role of Ag(I) and AgENMs in altering ZF protein function. To assess Zn(II) displacement from the ZF peptides, FluoZin-3, a Zn(II)-sensitive fluorescence probe was used (**Figure 6**). FluoZin-3 exhibits a dramatic increase in fluorescence in response to free Zn(II) in solution.[54] Moreover, it is far more responsive to Zn(II) than Ag(I). Control experiments were performed to ensure that Ag(I) and AgENMs did not react with FluoZin-3 and to ensure that Zn(II) was fully bound to the ZF peptides prior to addition of silver (**Figure SI.3**). To ease comparisons, all data in Figure 6 is shown as % change from the FluoZin-3 fluorescence recorded for the Zn(II)-bound ZF peptide without the addition of Ag(I) or AgENMs. Given the sensitivity of FluoZin-3 for free-Zn(II) and specificity for Zn(II) over Ag(I), it serves a rapid, sensitive method to detect displacement and release of Zn(II) from the ZF peptides.[28] The assay is a broadly applicable tool to directly probe for Zn(II) release upon metal ion substitution; a traditionally challenging experiment because Zn(II) is spectroscopically silent.

For both ZF peptides, the addition of one equivalent of Ag(I) results in a ~40-50% rise in FluoZin-3 fluorescence compared to that of Zn(II)-bound ZF peptides alone. From this increase in fluorescence, we conclude that the addition of Ag(I) results in Zn(II) ejection from the ZFs, at the very least results in the formation of a Zn(II)-bound complex that allows the dye to strip the Zn(II) from the binding pocket, despite the relatively low affinity of FluoZin-3 for Zn(II). This result is remarkably consistent with the observation of a ~40-50% loss of trypophan fluorescence upon addition of the same amount of Ag(I), as discussed in the previous section.

The addition of AgENMs to the Zn(II)-bound ZF peptides resulted in a ~70 % uniform change. Although it is hard to compare Ag(I) results directly to those from AgENMs, the release of Zn(II)

from the ZF peptides was similar across both AgENMs, independent of size. The concentrations of 10 and 40 nm AgENM used here were normalized to ensure consistent surface area, suggesting available surface area was key to determining Zn(II) release from the peptide.

In a cellular environment, release of Zn(II) from ZF proteins would not only disrupt ZF function, but also alter Zn(II) homeostasis. Changes in Zn(II) speciation, whether protein bound or unbound, may impact cell function beyond ZF, including zinc sensing, signaling, and complexation with low molecular weight biomolecules.[55]

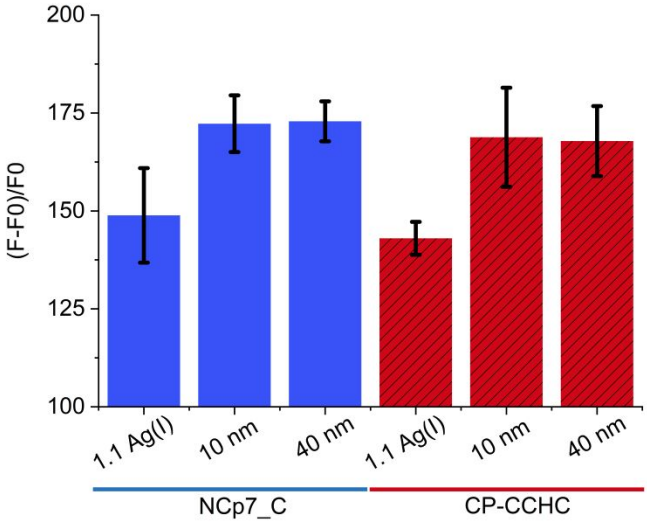

Figure 6. Relative change in fluorescence of FluoZin-3 after each of the following was added to 20 μM Zn(II) ZF peptide: 20 μM Ag(I), 0.0187 nM 10 nm AgENMs, and 0.001165 nM 40 nm AgENMs. Results are plotted as fluorescence changes relative to the respective, ion-free Zn(II)-bound ZF sample and expressed as (F-Fo)/Fo, where F is the fluorescence intensity of the sample with addition of a silver species and Fo is the fluorescence intensity of the Zn(II)-bound ZF sample, NCp7_C or CP-CCHC respectively. Samples were allowed to react with the silver species for 30 min before spectra were taken.

3.4. Changes to ZF peptide structure as a result of Ag(I) and AgENM interaction

ZF proteins and peptides rely upon a notable structural change upon Zn(II) binding to turn on cellular signaling functions. Only in the Zn(II) bound structure can ZF proteins bind DNA to regulate transcription, for example. Thus, ZF peptide structure changes upon addition of Ag(I) and AgENM provides insight into potential changes in ZF cellular function.

CD spectra were recorded to monitor structural changes to the Zn(II)-bound ZF peptides (**Figure 7**). Spectra of apo- and Zn(II) ZF peptides were recorded as comparisons, to assess the structural changes in each Zn(II)-bound ZF peptide upon addition of Ag(I) and AgENMs.

The addition of 1.1 equivalents of Ag(I) to Zn(II)-bound ZF peptides caused only minor changes to the Zn(II)-bound NCp7_C signature spectrum, the CP-CCHC spectrum most closely resembles that of the disordered apo-peptide with a spectral minimum at 198 nm. However,

upon addition of additional Ag(I), the NCp7_C spectrum overlays with the apo-NCp7_C spectrum, thus reinforcing the observation that higher stoichiometric ratios of Ag(I) are required alter the peptide, as observed in the UV-vis and tryptophan fluorescence studies. Because CD is an insensitive technique, we are unable to draw detailed insight into the structure of the peptide upon Ag(I) addition. However, the CD data for both ZF peptides indicate that addition of Ag(I) to the Zn(II)-bound structure results in a disordered peptide structure, and by extension, is likely to disrupt function.

The addition of AgENMs, whether 10 or 40 nm, to Zn(II)-bound ZF peptides, resulted in spectra that resemble the apo-peptide spectrum for both ZF peptides. For NCp7_C, the CD spectrum after addition of either AgENM overlaps with the apo-peptide indicating a random coil formation. For CP-CCHC, the CD spectra after addition of AgENMs have a wider shape but have a spectral minimum at 198 nm that is indicative of the apo-structure. Likely, the CP-CCHC peptide has a new, or hybridized structure (similar to both the apo- and Zn(II)-bound structures) after AgENM addition. Again, the spectral changes upon AgENM addition are indicative of changes to the structure of both ZFs, which is likely to disrupt function.

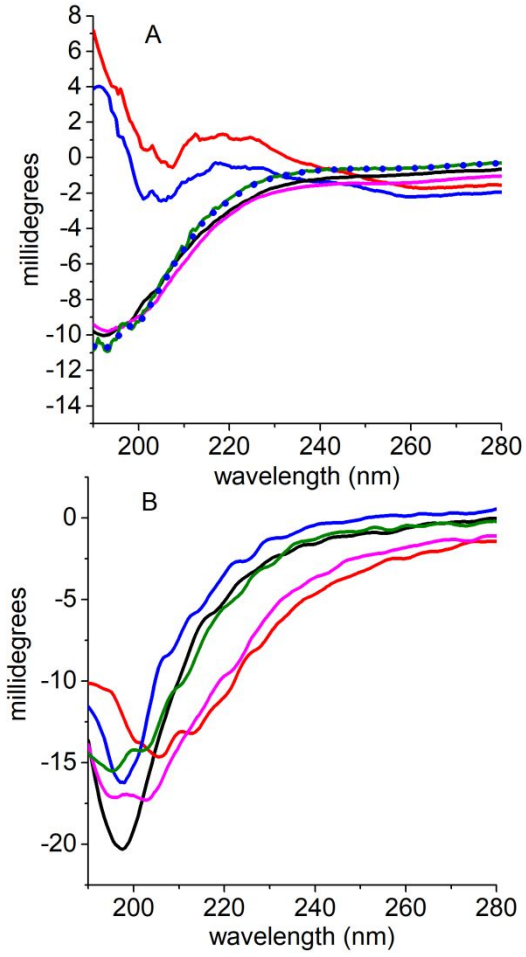

Figure 7. CD spectra of NCp7_C (A.) and CP-CCHC (B.) in reaction with Ag(I) and Ag ENMs. After recording the apo-peptide spectrum (black), Zn(II) was added and a Zn(II) peptide spectrum was obtained (red). To the Zn(II) peptide, the following silver species were added and spectra recorded: 1.1 ratio of Ag(I) (blue), 4.4 ratio of Ag(I) (blue dotted in A only), 10 nm Ag ENMs (pink), or 40 nm Ag ENMs (green) was added prior to taking a final spectrum of the sample. All spectra are of 20 μM peptide in 10 mM Tris buffer, pH 7.4.

5. Conclusion

To extend our understanding of the role of proteins in mediating AgENM transformation and cellular responses, we evaluated the interaction between AgENMs of two sizes with two model ZF peptides. Importantly, these ZF peptides do not differ in Zn(II) binding residues, but rather primary and secondary structural elements. Thus, by comparison of results across two different ZF peptides, we can ensure our results can be applied across an array of ZF structures. Our motivation in evaluating this system is broadly two-fold. First, to assess the impact of metalloproteins with exposed or label metal binding sites on AgENM transformations. Second, to specifically characterize ZF peptide structural changes as a result of AgENM and its dissolution product Ag(I). Since ZFs exhibit exposed metal binding sites and high metal binding constants, they are relevant models to test the ability of Ag(I) and AgENM disruption of metalloprotein sites. Any disruption of the metal binding and structure could have wide-ranging impacts on the transcriptional regulation in organisms iand provide mechanisms for AgENM cellular response.

Schematics summarizing insights into the interaction of AgENM and Ag(I) with apo- and Zn(II)-bound ZFs are summarized in **Figure 8**. In a high level overview, ZF peptides drive AgENM agglomeration and catalyze oxidative dissolution to form Ag(I). In turn, the native Zn(II) is displaced from the ZF peptides, if bound. The resulting peptide structure resembles the structure of the apo-ZF peptide. Spectroscopic studies show the apo-peptide, in the presence of Ag(I), can bind to the non-native metal to form Ag(I)-bound ZF peptides. Findings are discussed in more detail below, including minor differences across the two AgENM sizes and two different ZF peptides.

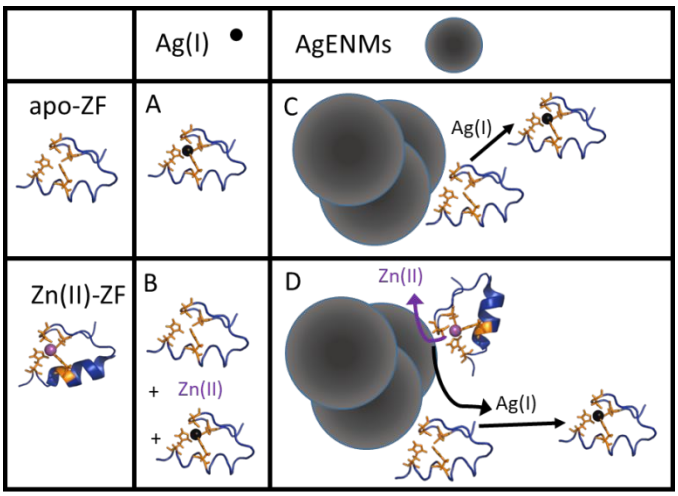

Figure 8. Schematic of ZF reaction with Ag(I) (small black sphere) and AgENMs (large grey spheres). (A.) Apo-ZFs react with Ag(I) to form Ag(I)-ZFs (Ag(I) shown as a black sphere in center of apo-structure). **(B.)** When Zn(II)-ZFs are reacted with Ag(I), the native Zn(II) (shown in purple) is displaced to form apo- and Ag(I)-bound ZFs and freely dissolved Zn(II). **(C.)** Reaction of apo-ZF with AgENMs leads to AgENM agglomeration and increased dissolution as AgENMs oxidize. Dissolved Ag(I) can bind to the apo-ZF to form Ag(I)-ZF. **(D.)** Interaction of AgENMs with Zn(II)-ZFs causes AgENM agglomeration and increased dissolution. The native Zn in Zn(II)-ZFs is displaced to form both apo-and Ag-bound forms of ZFs, which both have an apo-like ZF structure.

ZF peptides interact with AgENMs (citrate coated, 10 and 40 nm) to mediate AgENM transformations in solution. As indicated by zeta-potential measurements, the ZF peptides sorb toto the AgENM surface and change the charge. In addition, AgENMs agglomerate in the presence of ZF peptides, as indicated by DLS and TEM imaging. Finally, the ZF peptides catalyzed oxidative dissolution of AgENMs to increase Ag(I) concentrations in solution by two orders of magnitude. Because Ag(I) mediates most biocidal effects of the particles, this mechanism of dissolution is a key consideration in defining cellular response to AgENMs and motivates the independent study of Ag(I) binding to ZF peptides as well. Although the concentrations of ZF peptides here are much higher than in the cell, these results highlight the importance of proteins, especially those with readily available metal binding amino acids,[48] to drive transformations of AgENMs.

Comparing results across the 10 and 40 nm AgENMs, the smaller AgENMs tended to form larger aggregates and showed evidence of even smaller AgENMs in TEM. This size dependent peptide mediated agglomeration and oxidative dissolution is, in many ways similar to trends observed in other AgENM-biomolecule interactions. Parallel studies of AgENM sulfidation and of AgENM interaction with Ag(I) binding peptides indicate that agglomeration, oxidative dissolution, and even reformation of new AgENMs[11,12] is possible. Although no direct evidence of AgENM reformation was observed in our studies, additional characterization after longer timelines of reaction may reveal this phenomenon.

In turn, AgENMs and their oxidative dissolution product Ag(I) alter the structure of ZF peptides as well. Both 10 and 40 nm AgENMs caused displacement and release of the native Zn(II) from the ZF peptides, as observed by FluoZin-3 experiments. In addition, Zn(II)-bound ZF peptides after addition of excess Ag(I) and AgENMs lose their ordered Zn(II) bound secondary structures and become disordered, similar to the apo-peptide. This disordered structure may even include oxidative coupling between peptides[11,12] and multiple Ag(I) bound. Further studies can elucidate these key structural details. The overall change in structure, however, indicates a loss of ZF function. This insight is relevant to AgENM cell response and is a relevant molecular level detail to studies that have identified ZF proteins within the ENM corona.[34,56]

The product of AgENM oxidative dissolution, Ag(I)(*aq*), readily binds to the apo-form of both ZF peptides as shown by UV-vis titration studies. The native Zn(II) can also be displaced, as shown by tryptophan fluorescence for NCp7_C and by through the use of a Zn(II) sensitive fluorophore FluoZin-3. Secondary structural studies suggest that the structure after Zn(II) displacement resembles the apo-form of the peptide. Given the importance of the ZF protein structure to cellular function, the conformational changes observed here imply an alteration of ZF cellular function as well. To the best of our knowledge, this is the first report of a “silver finger” formation and extends the lengthening list of heavy metals with demonstrated interactions with ZF proteins.[57,58] Given the importance of ZF proteins to cellular signaling[58–60] and their readily accessible cysteines[48], future studies of metal and metaloxide ENMs should include structural elucidation of the Ag-bound peptide and assessment of ZF function *in vivo.*

Comparing the results across the two ZF peptides, CP-CCHC and NCp7_C, reveals the subtleties of peptide biophysical properties in mediating AgENM interactions. The slightly higher positive charge of CP-CCHC resulted in a higher zeta-potential and increased agglomeration when compared to NCp7_C. Yet, due to their similarity in metal binding amino acids, both apo-peptides readily bound Ag(I) and formed an apo-like structure upon interaction with AgENMs. Although the metal binding amino acids may dominate reactivity to homogenize the results across these two ZF peptides, these minor differences in reactivity between the two peptides suggest additional study of peptide-ENM interactions could reveal more on the biophysical features that drive protein and ENM transformations.

Given the sensitivity of these ZF peptides to Ag(I) and AgENMs, attention to ZFs and ZF signaling pathways deserves additional scrutiny when evaluating the cellular response and mechanisms of toxicity for metal and metal oxide nanomaterials. In addition, it is noteworthy that roughly 10% of the human genome consists of Zn(II) binding proteins.[59] With the biological diversity of structure and function in Zn(II)-binding domains, the impact of Ag and other metal / metaloxide ENMs on the structure and function of other Zn(II) binding domains deserves further study.

6. Acknowledgements

This research was supported by the National Institute of Environmental Health Sciences of the National Institutes of Health awarded to K.E.W. under award number R15ES025929. SCU student

research fellowships also supported this work, including support to M.E. from a Clare Boothe Luce fellowship, Z.N.A. by a DeNardo Award, and K.B. by Hayes Award. The authors would like to thank Austin M. Cole (UC Davis Interdisciplinary Center for Plasma Mass Spectrometry (UCD/ICPMS), a Campus Research Core Facility (CRCF) for technical assistance and ICP-MS data. The ICP-MS data was collected using an Agilent 8900 ICP-MS purchased with funding from the UC Davis Research Core Facilities Program's (RCFP's) CRCF Enhancement Funding Program managed by the UC Davis Office of Research (UCD OR). Finally, warm thanks to Kris McNeill and group at ETH-Zurich, who provided K.E.W. a sabbatical home while much of this manuscript was written.

6. References

(1) Vance, M. E.; Kuiken, T.; Vejerano, E. P.; McGinnis, S. P.; Hochella, M. F.; Hull, D. R. Nanotechnology in the Real World: Redeveloping the Nanomaterial Consumer Products Inventory. *Beilstein J. Nanotechnol.* **2015**, *6* (1), 1769–1780.

(2) Reidy, B.; Haase, A.; Luch, A.; Dawson, K.; Lynch, I. Mechanisms of Silver Nanoparticle Release, Transformation and Toxicity: A Critical Review of Current Knowledge and Recommendations for Future Studies and Applications. *Materials (Basel).* **2013**, *6* (12), 2295–2350.

(3) Marambio-Jones, C.; Hoek, E. M. V. A Review of the Antibacterial Effects of Silver Nanomaterials and Potential Implications for Human Health and the Environment. *J. Nanoparticle Res.* **2010**, *12* (5), 1531–1551.

(4) Eckhardt, S.; Brunetto, P. S.; Gagnon, J.; Priebe, M.; Giese, B.; Fromm, K. M. Nanobio Silver: Its Interactions with Peptides and Bacteria, and Its Uses in Medicine. *Chem. Rev.* **2013**, *113* (7), 4708–4754.

(5) Johnston, H. J.; Hutchison, G.; Christensen, F. M.; Peters, S.; Hankin, S.; Stone, V. A Review of the in Vivo and in Vitro Toxicity of Silver and Gold Particulates: Particle Attributes and Biological Mechanisms Responsible for the Observed Toxicity. *Crit. Rev. Toxicol.* **2010**, *40* (4), 328–346.

(6) De Paoli Lacerda, S. H.; Park, J. J.; Meuse, C.; Pristinski, D.; Becker, M. L.; Karim, A.; Douglas, J. F. Interaction of Gold Nanoparticles with Common Human Blood Proteins. *ACS Nano* **2009,** *4* (1), 365-79.

(7) Ji, J. H.; Jung, J. H.; Kim, S. S.; Yoon, J.-U.; Park, J. D.; Choi, B. S.; Chung, Y. H.; Kwon, I. H.; Jeong, J.; Han, B. S.; et al. Twenty-Eight-Day Inhalation Toxicity Study of Silver Nanoparticles in Sprague-Dawley Rats. *Inhal. Toxicol.* **2007**, *19* (10), 857–871.

(8) Park, K.; Park, E.-J.; Chun, I. K.; Choi, K.; Lee, S. H.; Yoon, J.; Lee, B. C. Bioavailability and Toxicokinetics of Citrate-Coated Silver Nanoparticles in Rats. *Arch. Pharm. Res.* **2011**, *34* (1), 153–158.

(9) Landsiedel, R.; Fabian, E.; Ma-Hock, L.; Wohlleben, W.; Wiench, K.; Oesch, F.; van Ravenzwaay, B. Toxico-/Biokinetics of Nanomaterials. *Arch. Toxicol.* **2012**, *86* (7), 1021–1060.

(10) Armstrong, N.; Ramamoorthy, M.; Lyon, D.; Jones, K.; Duttaroy, A. Mechanism of Silver Nanoparticles Action on Insect Pigmentation Reveals Intervention of Copper Homeostasis. *PLoS One* **2013**, *8* (1), e53186.

(11) Vasylevskyi, S. I.; Kracht, S.; Corcosa, P.; Fromm, K. M.; Giese, B.; Füeg, M. Formation of Silver Nanoparticles by Electron Transfer in Peptides and C-Cytochromes. *Angew. Chemie Int. Ed.* **2017**, *56* (21), 5926–5930.

(12) Kracht, S.; Messerer, M.; Lang, M.; Eckhardt, S.; Lauz, M.; Grobéty, B.; Fromm, K. M.; Giese, B. Electron Transfer in Peptides: On the Formation of Silver Nanoparticles. *Angew. Chemie Int. Ed.* **2015**, *54* (10), 2912–2916.

(13) Martinolich, A. J.; Park, G.; Nakamoto, M. Y.; Gate, R. E.; Wheeler, K. E. Structural and Functional Effects of Cu Metalloprotein-Driven Silver Nanoparticle Dissolution. *Environ. Sci. Technol.* **2012**, *46* (11), 6355–6362.

(14) Freitas, D. N.; Martinolich, A. J.; Amaris, Z. N.; Wheeler, K. E. Beyond the Passive Interactions at the Nano-Bio Interface: Evidence of Cu Metalloprotein-Driven Oxidative Dissolution of Silver Nanoparticles. *J. Nanobiotechnology* **2016**, *14* (1), 7.

(15) Liu, W.; Worms, I. A. M.; Herlin-Boime, N.; Truffier-Boutry, D.; Michaud-Soret, I.; Mintz, E.; Vidaud, C.; Rollin-Genetet, F. Interaction of Silver Nanoparticles with Metallothionein and Ceruloplasmin: Impact on Metal Substitution by Ag(I), Corona Formation and Enzymatic Activity. *Nanoscale* **2017**, *9*, 6581-6594 .

(16) Zelazowski, A. J.; Stillman, M. J. Silver Binding to Rabbit Liver Zinc Metallothionein and Zinc α and β Fragments. Formation of Silver Metallothionein with Ag(I): Protein Ratios of 6, 12, and 18 Observed Using Circular Dichroism Spectroscopy. *Inorg. Chem.* **1992,** *264* (29), 17091-9.
(17) Käkinen, A.; Ding, F.; Chen, P.; Mortimer, M.; Kahru, A.; Ke, P. C. Interaction of Firefly Luciferase and Silver Nanoparticles and Its Impact on Enzyme Activity. *Nanotechnology* **2013**, *24* (34), 345101.
(18) Durán, N.; Silveira, C. P.; Durán, M.; Martinez, D. S. T. Silver Nanoparticle Protein Corona and Toxicity: A Mini-Review. *J. Nanobiotechnology* **2015**, *13* (1), 55.
(19) Ostermeyer, A.-K.; Kostigen Mumuper, C.; Semprini, L.; Radniecki, T. Influence of Bovine Serum Albumin and Alginate on Silver Nanoparticle Dissolution and Toxicity to *Nitrosomonas Europaea*. *Environ. Sci. Technol.* **2013**, *47* (24), 14403–14410.
(20) Berg, J. M.; Godwin, H. A. Lessons from Zinc-Binding Peptides. *Annu. Rev. Biophys. Biomol. Struct* **1997**, *26*, 357–371.
(21) Laity, J. H.; Lee, B. M.; Wright, P. E. Zinc Finger Proteins: New Insights into Structural and Functional Diversity. *Current Opinion in Structural Biology*. 2001.
(22) Lee, S. J.; Michel, S. L. J. Structural Metal Sites in Nonclassical Zinc Finger Proteins Involved in Transcriptional and Translational Regulation. *Acc. Chem. Res.* **2014**, *47* (8), 2643–2650.
(23) DiTargiani, R. C.; Lee, S. J.; Wassink, S.; Michel, S. L. J. Functional Characterization of Iron-Substituted Tristetraprolin-2D (TTP-2D, NUP475-2D): RNA Binding Affinity and Selectivity. *Biochemistry* **2006,** *45* (45):13641-9.
(24) Krizek, B. A.; Berg, J. M. Complexes of Zinc Finger Peptides with Nickel(2+) and Iron(2+). *Inorg. Chem.* **1992**, *31* (13), 2984–2986.
(25) Bal, W.; Schwerdtle, T.; Hartwig, A. Mechanism of Nickel Assault on the Zinc Finger of DNA Repair Protein XPA. *Chem. Res. Toxicol.* **2003**, *16(2)*, 242-248.
(26) Franzman, M. A.; Barrios, A. M. Spectroscopic Evidence for the Formation of Goldfingers. *Inorg. Chem.* **2008,** *47* (10), 3928-30.
(27) Larabee, J. L.; Hocker, J. R.; Hanas, J. S. Mechanisms of Aurothiomalate-Cys2His2 Zinc Finger Interactions. *Chem. Res. Toxicol.* **2005,** *18* (12), 1943-54.
(28) Doku, R. T.; Park, G.; Wheeler, K. E.; Splan, K. E. Spectroscopic Characterization of Copper(I) Binding to Apo and Metal-Reconstituted Zinc Finger Peptides. *J Biol Inorg Chem* 2013, *18* (6), 669-78.
(29) Liang, Y.; Ewing, P. M.; Laursen, W. J.; Tripp, V. T.; Singh, S.; Splan, K. E. Copper-Binding Properties of the BIR2 and BIR3 Domains of the X-Linked Inhibitor of Apoptosis Protein. *J. Inorg. Biochem.* **2014**, *140*, 104–110.
(30) Shimberg, G. D.; Ok, K.; Neu, H. M.; Splan, K. E.; Michel, S. L. J. Cu(I) Disrupts the Structure and Function of the Nonclassical Zinc Finger Protein Tristetraprolin (TTP).
(31) Michalek, J. L.; Lee, S. J.; Michel, S. L. J. J. Cadmium Coordination to the Zinc Binding Domains of the Non-Classical Zinc Finger Protein Tristetraprolin Affects RNA Binding Selectivity. *J. Inorg. Biochem.* **2012**, *112*, 32–38.
(32) Krizek, B. A.; Merkle, D. L.; Berg ', J. M. Ligand Variation and Metal Ion Binding Specificity in Zinc Finger Peptidest. *Inorg. Chem* **1993**, *32*, 937–940.
(33) Payne, J. C.; Ter Horst, M. A.; Godwin, H. A. Lead Fingers: Pb2+ Binding to Structural Zinc-Binding Domains Determined Directly by Monitoring Lead-Thiolate Charge-Transfer Bands. *J. Am. Chem. Soc.* **1999**, *121* (13), 6850–6855.
(34) Eigenheer, R.; Castellanos, E. R.; Nakamoto, M. Y.; Gerner, K. T.; Lampe, A. M.; Wheeler, K. E. Silver Nanoparticle Protein Corona Composition Compared across Engineered Particle Properties and Environmentally Relevant Reaction Conditions. *Environ. Sci. Nano* **2014**, *1* (3), 238.
(35) Walkey, C. D.; Olsen, J. B.; Song, F.; Liu, R.; Guo, H.; Olsen, D. W. H.; Cohen, Y.; Emili,

A.; Chan, W. C. W. W. Protein Corona Fingerprinting Predicts the Cellular Interaction of Gold and Silver Nanoparticles. *ACS Nano* **2014**, *8* (3), 2439–2455.
(36) Bird, A. J.; McCall, K.; Kramer, M.; Blankman, E.; Winge, D. R.; Eide, D. J. Zinc Fingers Can Act as Zn2+ Sensors to Regulate Transcriptional Activation Domain Function. *EMBO J.* **2003**, *22* (19), 5137–5146.
(37) Chang, C. J. Searching for Harmony in Transition-Metal Signaling. *Nat. Chem. Biol. 2015 1110* **2015**.
(38) Krizek, B. A.; Amann, B. T.; Kilfoil, V. J.; Merkle, D. L.; Berg, J. M. A Consensus Zinc Finger Peptide: Design, High-Affinity Metal Binding, a PH-Dependent Structure, and a His to Cys Sequence Variant. *J. Am. Chem. SOC* **1991**, *113*, 4518–4523.
(39) Sénèque, O.; Latour, J. M. Coordination Properties of Zinc Finger Peptides Revisited: Ligand Competition Studies Reveal Higher Affinities for Zinc and Cobalt. *J. Am. Chem. Soc.* **2010**, *132* (1), 17760–17774.
(40) Darlix, J.-L.; Lapadat-Tapolsky, M.; de Rocquigny, H.; Roques, B. P. First Glimpses at Structure-Function Relationships of the Nucleocapsid Protein of Retroviruses. *J. Mol. Biol.* **1995**, *254* (4), 523–537.
(41) South, T. L.; Blake, P. R.; Hare, D. R.; Summers, M. F. C-Terminal Retroviral-Type Zinc Finger Domain from the HIV-1 Nucleocapsid Protein Is Structurally Similar to the N-Terminal Zinc Finger Domain? *Biochemistry* **1991**, *30*, 6342–6349.
(42) E. Bombarda, ‡; H. Cherradi, ‡; N. Morellet, §; B. P. Roques, § and; Y. Mély*, ‡. Zn2+ Binding Properties of Single-Point Mutants of the C-Terminal Zinc Finger of the HIV-1 Nucleocapsid Protein: Evidence of a Critical Role of Cysteine 49 in Zn2+ Dissociation†. **2002,** 41(13):4312-20.
(43) Mély, Y.; De Rocquigny, H.; Morellet, N.; Roques, B. P.; Gérard, D.; M??ly, Y.; De Rocquigny, H.; Morellet, N.; Roques, B. P.; G??rard, D. Zinc Binding to the HIV-1 Nucleocapsid Protein: A Thermodynamic Investigation by Fluorescence Spectroscopy. *Biochemistry* **1996**.
(44) Riddles, P. W.; Blakeley, R. L.; Zerner, B. Reassessment of Ellman's Reagent. *Methods Enzymol.* **1983**, *91* (C), 49–60.
(45) Dennison, J. M.; Zupancic, J. M.; Lin, W.; Dwyer, J. H.; Murphy, C. J. Protein Adsorption to Charged Gold Nanospheres as a Function of Protein Deformability. *Langmuir* **2017**, *33* (31), 7751–7761.
(46) Loza, K.; Diendorf, J.; Sengstock, C.; Ruiz-Gonzalez, L.; Gonzalez-Calbet, J. M.; Vallet-Regi, M.; Köller, M.; Epple, M. The Dissolution and Biological Effects of Silver Nanoparticles in Biological Media. *J. Mater. Chem. B* **2014**, *2* (12), 1634–1643.
(47) Liu, J.; Pennell, K. G.; Hurt, R. H. Kinetics and Mechanisms of Nanosilver Oxysulfidation. *Environ. Sci. Technol.* **2011**, *45* (17), 7345–7353.
(48) Marchioni, M.; Gallon, T.; Worms, I.; Jouneau, P.-H.; Lebrun, colette; Veronesi, G.; Truffier-Boutry, D.; Mintz, E.; Delangle, P.; Deniaud, A.; et al. Insights into Polythiol-Assisted AgNP Dissolution Induced by Bio-Relevant Molecules. *Environ. Sci. Nano* **2018, 5**, 1911-1920.
(49) Chabert, V.; Hologne, M.; Sénèque, O.; Crochet, A.; Walker, O.; Fromm, K. M. Model Peptide Studies of Ag $^{+}$ Binding Sites from the Silver Resistance Protein SilE. *Chem. Commun.* **2017**, *53* (45), 6105–6108.
(50) Thalmann, B.; Voegelin, A.; Sinnet, B.; Morgenroth, E.; Kaegi, R. Sulfidation Kinetics of Silver Nanoparticles Reacted with Metal Sulfides. *Environ. Sci. Technol.* **2014**, *48* (9), 4885–4892.
(51) Levard, C.; Hotze, E. M.; Lowry, G. V.; Brown, G. E. Environmental Transformations of Silver Nanoparticles: Impact on Stability and Toxicity. *Environ. Sci. Technol.* **2012**, *46* (13), 6900–6914.
(52) Zhang, W.; Xiao, B.; Fang, T. Chemical Transformation of Silver Nanoparticles in Aquatic

Environments: Mechanism, Morphology and Toxicity. *Chemosphere* **2018**, *191*, 324–334.
(53) Angeletti, B.; Waldron, K. J.; Freeman, K. B.; Bawagan, H.; Hussain, I.; Miller, C. C. J.; Lau, K.-F.; Tennant, M. E.; Dennison, C.; Robinson, N. J.; et al. BACE1 Cytoplasmic Domain Interacts with the Copper Chaperone for Superoxide Dismutase-1 and Binds Copper. *J. Biol. Chem.* **2005**, *280* (18), 17930–17937.
(54) Domaille, D. W.; Que, E. L.; Chang, C. J. Synthetic Fluorescent Sensors for Studying the Cell Biology of Metals. *Nat. Chem. Biol.* **2008**, *4* (3), 168–175.
(55) Krężel, A.; Maret, W. The Biological Inorganic Chemistry of Zinc Ions. *Arch. Biochem. Biophys.* **2016**, *611*, 3–19.
(56) Walkey, C. D.; Olsen, J. B.; Song, F.; Liu, R.; Guo, H.; Olsen, D. W. H.; Cohen, Y.; Emili, A.; Chan, W. C. W. Protein Corona Fingerprinting Predicts the Cellular Interaction of Gold and Silver Nanoparticles. *ACS Nano* **2014**, *8* (3), 2439–2455.
(57) Günther, V.; Lindert, U.; Schaffner, W. The Taste of Heavy Metals: Gene Regulation by MTF-1. *Biochim. Biophys. Acta - Mol. Cell Res.* **2012**, *1823* (9), 1416–1425.
(58) Zawia N.H., Razmiafshari M. (2002) Elucidation of the Zinc-Finger Motif as a Target for Heavy-Metal Perturbations. In: Massaro E.J. (eds) Handbook of Neurotoxicology. Humana Press, Totowa, NJ.
(59) Andreini, C.; Banci, L.; Bertini, I.; Rosato, A. Counting the Zinc-Proteins Encoded in the Human Genome. *J. Proteome Res.* **2006,** *5* (1),196-201.
(60) Witkiewicz-Kucharczyk, A.; Bal, W. Damage of Zinc Fingers in DNA Repair Proteins, a Novel Molecular Mechanism in Carcinogenesis. *Toxicol. Lett.* **2006**, *162* (1 SPEC. ISS.), 29–42.

7. Supplemental Information

SI.1. Histograms of TEM size measurements

SI.2. Aqueous silver titrations into buffer and ZF peptides in water

SI.3. FluoZin3 control results

TOC art